Soft Matter

Slip and momentum transfer mechanisms mediated by Janus rods at polymer interfaces

Journal:	*Soft Matter*
Manuscript ID	SM-ART-05-2020-000858.R1
Article Type:	Paper
Date Submitted by the Author:	18-Jun-2020
Complete List of Authors:	Paiva, Felipe; Case Western Reserve University, Macromolecular Science and Engineering; Universidade Federal do Rio de Janeiro, School of Chemistry Resende, Argimiro; Universidade Federal do Rio de Janeiro, Laboratório de Modelagem, Simulação e Controle de Processos Químicos. Programa de Engenharia Química/COPPE Calado, Veronica; Universidade Federal do Rio de Janeiro, School of Chemistry Maia, Joao; Case Western Reserve University, Macromolecular Science and Engineering Khani, Shaghayegh; Case Western Reserve University, Macromolecular Science and Engineering

Soft Matter

ROYAL SOCIETY OF CHEMISTRY

ARTICLE TYPE

Cite this: DOI: 10.1039/xxxxxxxxxx

Slip and momentum transfer mechanisms mediated by Janus rods at polymer interfaces†

Felipe L. Paiva,[a,b] Argimiro R. Secchi,[c] Verônica Calado,[a] João Maia,[*,b] and Shaghayegh Khani[*,b]

Received Date
Accepted Date

DOI: 10.1039/xxxxxxxxxx

www.rsc.org/journalname

As an incipient but preeminent technology for multiphase nanomaterials/fluids, exact compatibilizing mechanisms of Janus particles in polymer blends and the consequent morphology remain unknown. The contributions of Janus nanorods to slip suppression and momentum transfer across the interface have been explored through Dissipative Particle Dynamics simulations under shear flow at unentangled polymer-polymer interfaces. Rods have been then grafted with flexible polymer chains to unveil interfacial structure-property relationships at a molecular level when compared with flexible diblock copolymer surfactants. When Janus rods are sparsely grafted with necessarily longer grafts, they favor a greater degree of graft interpenetration with polymer phases. This yields less effective momentum transfer that impacts droplet coalescence processes; dynamic heterogeneities at complex interfaces; and helps map their efficiency as compatibilizers.

1 Introduction

Whether it is for coextrusion or blending processes;[1,2] adhesive properties;[3–5] or rheological properties in general,[1,5–8] the study of polymer-polymer interfaces is paramount in various applications involving multiphase polymeric materials. An understanding of dynamic interfacial phenomena in mixtures of polymers at the molecular scale helps design the mechanical or tribological properties of nanostructured materials.[9–13] This is for example the case in nanometrically confined flows and nanodevices.[14,15]

Among the structure-property relationships between interfacial structure and mechanics of polymer systems, interfacial slip has been studied since the seminal scaling predictions by de Gennes and coworkers.[16–19] Since then, their scaling predictions for unentangled polymer interfaces have been verified by Goveas and Fredrickson;[20] Barsky and Robbins;[21] and by Narayanan *et al.*[22] Controlling the extent of slip is naturally important for technological applications, and block copolymers can be used for this purpose.[22,23] In that sense, Narayanan *et al.*[22] investigated the role of block copolymer compatibilizers in suppressing slip as this had been experimentally verified by Zhao and Macosko.[1] Narayanan *et al.*[22] additionally assessed how block copolymers compose an interfacial layer of effectively higher viscosity in comparison with the bulk polymer viscosities.[22] In turn, this higher energy dissipation rate at the interface makes the film drainage time between two colliding droplets increase significantly.[22] This would then contribute to inhibit droplet coalescence and is in agreement with experimental observations.[24–27] It also makes for a good example of how molecular simulations are able to more easily unveil the underlying physics of global experimental trends.

Guo *et al.*[28] verified that flow-induced droplet coalescence is correlated with how easily polymer chains are stretched in response to an external shear stress, specially at an interfacial level. This also applied to extant compatibilizers that contribute to enhanced "friction" or higher viscosity at the interface.[28] However, in that study, the molecular architecture of the compatibilizer was kept fixed and relatively simple. Very recently, and similarly to the effects verified by Narayanan *et al.*[22] and Guo *et al.*,[28] Sagis *et al.*[29] combined experimental and Molecular Dynamics (MD) computational efforts to illustrate how block copolymers and the more viscous interfacial layer make for less effective momentum transfer across the interface. This momentum transfer mechanism, according to the authors,[29] is responsible for observed dynamic heterogeneities at interfaces containing nanoparticles, polymers, and proteins in step extension-compression experiments. The mechanism of less efficient momentum transfer provided by block copolymers seems to have been, in the au-

[a] School of Chemistry, Universidade Federal do Rio de Janeiro, Rua Horácio Macedo 2030, Cidade Universitária, Rio de Janeiro, RJ 21941-909, Brazil.
[b] Department of Macromolecular Science and Engineering, Case Western Reserve University, 2100 Adelbert Road, Cleveland, OH 44106, USA.
[c] Chemical Engineering Graduate Program (COPPE), Universidade Federal do Rio de Janeiro, Rua Horácio Macedo 2030, Cidade Universitária, Rio de Janeiro, RJ 21941-909, Brazil.
* E-mail: joao.maia@case.edu; shaghayegh.khani@case.edu.

† Electronic Supplementary Information (ESI) available: fitted density and velocity profiles; polymer chain end concentration; effects of surfactants on interfacial width/penetration; effects of modified DPD weight functions; surfactant orientation and diffusion; block copolymer snapshots; and bulk/interfacial shear stress calculations. See DOI: 10.1039/cXsm00000x/

thors' own words,[29] overlooked by interfacial rheology practitioners over the years. In other words, it was not until recently that the effects observed by Narayanan *et al.*[22] and Guo *et al.*[28] were found to play a central role in dictating dynamic heterogeneities at more complex interfaces. These observations and remarks urge for a better understanding of how complex interfaces and momentum transfer are related and this is a topic to which the present work aims to contribute.

Janus particles[30] are more interfacially active than commonly-used flexible block copolymer surfactants.[31] In general, Janus particles have been found to better stabilize morphologies and reduce interfacial tension to a greater extent than block copolymers, even though there are some intricacies that have been recently found to apply.[32–34] As an illustration of these findings, enhanced Van der Waals (VDW) interactions between metal particle cores seem to make for reduced film drainage times between colliding polymeric droplets.[34,35] Therefore, in this case, block copolymers would be better stabilizers than Janus particles in spite of lower interfacial tension provided by Janus particles.[34,35] Other factors would also have to be present to explain these significant reductions in film drainage times that may be observed with nanoparticles, such as sufficiently high interfacial diffusivity; high nanoparticle concentration; and/or the structure of the polymeric corona surrounding the nanoparticle.[34,35] In any case, the exact mechanisms through which Janus particles may stabilize emulsions, for example, are far from elucidated. This is also a shortcoming that the present work intends to help clarify.

Herein, a distinctive and largely unexplored aspect of Janus surfactants is examined. In particular, a tangential shear flow is applied at a planar polymer-polymer interface to investigate specifically how Janus particles affect interfacial slip and mediate momentum transfer across the interface. The interface contains either flexible block copolymers or bare/polymer-coated Janus rods so that meaningful comparisons can be made. As highlighted recently by Cardinaels,[36] this is important as the neat blend is mostly taken to be the reference case in Janus-related studies, which makes direct comparisons with copolymers rather scarce. Rigid Janus rods are grafted with flexible chains to show how grafting density – number of grafts N_g – and graft chain length L_g influence slip and shear interfacial viscosity. The effects of these parameters on interfacial 2D structure have also been evaluated. While plenty of studies exist regarding the effects of L_g and N_g on homogeneous nanorod assembly,[37–41] how these parameters affect the interfacial assembly of polymer-grafted Janus nanorods is presently unknown. The Schmidt number (Sc) associated with the present Dissipative Particle Dynamics (DPD) simulations is accordingly increased to show how conclusions pertaining to momentum transfer are likely not subject to the typically low Sc of DPD simulations. The present mesoscale assessment of momentum transfer efficiency across polymer-polymer interfaces provides molecular-level insight that may guide droplet coalescence studies.[24–27] It also more clearly unveils mechanisms governing dynamic heterogeneities[29] and mechanics at polymer-polymer interfaces with more complex Janus compatibilizers.

2 Simulation model

DPD is a particle-based, coarse-grained simulation technique first introduced by Hoogerbrugge and Koelman.[42] In that work and in a series of subsequent papers,[43,43–45] the authors laid out the hydrodynamic equations and statistical mechanics of this simulation method that conserves momentum and mass.[44] The dynamics of a DPD fluid are described by a stochastic term that introduces thermal Brownian motion in the system and by a damping term that plays the role of viscous forces and is the heat sink of the system. Hence, DPD encompasses the use of a random force $\mathbf{F_{ij}^R}$ (Equation 1) and a dissipative force $\mathbf{F_{ij}^D}$ (Equation 2) to describe correct thermodynamic equilibrium between neighboring particles i and j that interact within a specific cut-off distance of r_c:

$$\mathbf{F_{ij}^R} = \frac{\Omega\omega^R(r_{ij})\theta_{ij}\hat{\mathbf{r}}_{\mathbf{ij}}}{\sqrt{\Delta t}} \tag{1}$$

$$\mathbf{F_{ij}^D} = -\gamma\omega^D(r_{ij})(\hat{\mathbf{r}}_{\mathbf{ij}}\cdot\mathbf{v_{ij}})\hat{\mathbf{r}}_{\mathbf{ij}} \tag{2}$$

where $\mathbf{v_{ij}} = \mathbf{v_i} - \mathbf{v_j}$ is the relative velocity; the dissipation strength is represented by γ; $\omega^D(r_{ij})$ and $\omega^R(r_{ij})$ are weight functions; Δt is a short time interval; the thermal noise corresponds to Ω; and θ_{ij} is a Gaussian random number with zero mean and unit variance.

Intermolecular interactions are normally treated with the use of a purely repulsive conservative force $\mathbf{F_{ij}^C}$ (Equation 3):

$$\mathbf{F_{ij}^C} = \begin{cases} a_{ij}(1-\frac{r_{ij}}{r_c})\hat{\mathbf{r}}_{\mathbf{ij}}; & r_{ij} < r_c \\ 0; & r_{ij} \geq r_c \end{cases} \tag{3}$$

where a_{ij} is the strength of the potential between particles; $\mathbf{r_{ij}} = \mathbf{r_i} - \mathbf{r_j}$ is the distance between these particles; $r_{ij} = |\mathbf{r_{ij}}|$; and $\hat{\mathbf{r}}_{\mathbf{ij}} = \frac{\mathbf{r_{ij}}}{|\mathbf{r_{ij}}|}$ is its unit vector. For simplicity, r_c is set to 1.0.

Taking into account these three forces, Newton's equation of motion is then solved for pairs of interacting particles according to the net force $\mathbf{F_i}$ acting on particle i (Equation 4):

$$\mathbf{F_i} = \sum_{i\neq j} \mathbf{F_{ij}^C} + \mathbf{F_{ij}^D} + \mathbf{F_{ij}^R} \tag{4}$$

where this has been done using a modified version of the velocity-Verlet algorithm.[46,47]

Español and Warren[45] showed thermodynamically how these terms have to be chosen carefully so that they compose a fluctuation-dissipation theorem and, thus, a Gibbs canonical NVT ensemble. The NVT thermostat[45] is formed according to Equations 5 and 6, where the weight functions $\omega^D(r_{ij})$ and $\omega^R(r_{ij})$ are most frequently used in the generalized form of Equation 6:

$$\Omega^2 = 2\gamma k_B T \tag{5}$$

$$\omega^D(r_{ij}) = \left[\omega^R(r_{ij})\right]^2 = \begin{cases} \left(1-\frac{r_{ij}}{r_c}\right)^s; & r_{ij} < r_c \\ 0; & r_{ij} \geq r_c \end{cases} \tag{6}$$

where T is the system's temperature; k_B is Boltzmann's constant; and s is an exponent that normally takes the value of 2. This s value has been used throughout the present work unless stated otherwise.

Additionally, adjacent monomeric units in polymer chains inter-

act via a spring force $\mathbf{F_{ij}^S}$ to simulate polymer bonds (Equation 7):

$$\mathbf{F_{ij}^S} = k^S(r_{ij} - r_{eq})\hat{\mathbf{r}}_{\mathbf{ij}} \quad (7)$$

where k^S is the spring constant and r_{eq} is the equilibrium bond length. These parameters are set respectively as $100\frac{k_BT}{r_c^2}$ and $0.85\ r_c$. Polymers A and B composing a symmetric blend are generated randomly, but in a way that they are in separate halves of the calculation box initially to increase computational efficiency. Likewise, all surfactant particles are generated initially already at the interfacial plane ($y = 0$) to decrease the computational cost linked with diffusion to the interface. The total number of DPD polymer particles in the system is kept constant at 16,000 in a cubic box of $48\ r_c \times 48\ r_c \times 48\ r_c$. The length C of polymer chains, however, varies so that the effect of polymer molar mass on interfacial slip can be evaluated. After an equilibration period of $1 \times 10^5\ \tau$, for measuring equilibrium properties, a data acquisition period of $2 \times 10^5\ \tau$ follows. For shear flow simulations, a shearing stage follows instead for $1 \times 10^5\ \tau$, identically to a recent study using the same model.[48] Shear flow is applied in the x direction using Lees-Edwards boundary conditions,[49–56] in a way that the velocity gradient direction is in the same direction as the normal of the interface (y direction). A shear rate $\dot{\gamma}$ of $0.07\ \tau^{-1}$ is used that corresponds to the nanorod tilting behavior observed in Paiva *et al.*[48] It corresponds to a translational Péclet number of 76 for a Janus rod with an aspect ratio (AR) of 2.0.[48] This shear rate is chosen so that conclusions are freed from the slightly more involved dynamic behavior presented by these rigid compatibilizers at higher shear rates.[48] Periodic boundary conditions are employed in all three directions and the time step is kept constant at $0.01\sqrt{\frac{mr_c^2}{k_BT}}$, where m is the mass of a DPD particle.

Model rigid surfactants utilized in the present work are exactly the same as previously published works.[37,48,57,58] Briefly, however, DPD particles are attached together linearly and one-dimensionally with a fixed distance ($0.2\ r_c$) between each other. This results in an effectively impenetrable one-dimensional object for which rigid body dynamics equations are solved.[46,59] These Janus rods (JR) are symmetrically amphiphilic and of various AR according to their length L and diameter d: $\frac{L}{d} = \frac{(N_R-1)(0.2d)}{d}$, where N_R is the number of DPD particles composing the Janus rod. Unless specified otherwise, JR have an aspect ratio of 2.0. Block copolymers are named as h5t5, h10t10 or h15t15 according to the corresponding number of head/tail groups. For example, 5 DPD particles in h5t5 are affine to one polymer phase; and 5 others are affine to the other phase. The differences between Janus and flexible surfactants are, thus, their various sizes and the fact that particles composing block copolymers interact via a spring force identical to the homopolymer phases. Then, nanorods are correspondingly grafted with flexible chains to prospect how the number/length of grafts influences not only interfacial microstructure, but also its interplay with momentum transfer across the interface. Graft particles on Janus rods interact via the very same spring force as flexible surfactants and homopolymer phases. Depending on how these particle chains are distributed along JR, this results in a different number of polymer grafts N_g each with a length L_g. The scheme in Figure 1 illustrates exactly where on the rod (AR=2.0) particles are grafted composing thus various grafting densities. Grafts are free to rotate around the long axis of nanorods. They then would correspond to relatively more mobile ligands[34,60] when for example a gold-sulfur interface is considered.[61]

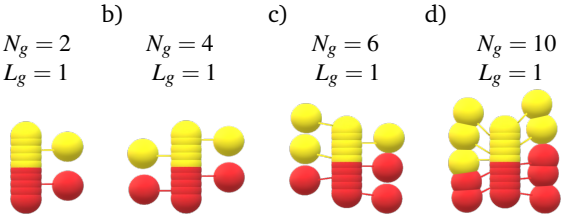

Fig. 1 Schematic representation of grafted Janus rods exhibiting various grafting densities with $L_g = 1$: a) $N_g = 2$; b) $N_g = 4$; c) $N_g = 6$; d) and $N_g = 10$. Even though the scheme is not drawn to scale, the rod particle onto which chains are grafted is appropriately represented. Rods are grafted symmetrically with respect to their amphiphilicity. The yellow portion represents the part that more favorably interacts with polymer A (J_A) and the red portion interacts more favorably with polymer B (J_B).

An equation of state can be derived from a top-down approach in which the underlying fluid is known and its compressibility is matched to that of the DPD fluid.[47] For water and a coarse-graining degree of 1.0, Equation 8 defines the relative strength of interaction potentials:[47]

$$\frac{a_{ij}\rho}{k_BT} = 75 \quad (8)$$

A density of $3.0\ r_c^{-3}$ has been used given that computing time increases with the density of particles in the calculation box. For simplicity, the energy scale is set to $k_BT = 1.0$ from $\gamma = 4.5$ and $\Omega = 3.0$ in Equation 5. This makes repulsion parameters for the soft interaction potentials in DPD be $a_{ij} = 25\ \frac{k_BT}{r_c}$ between like species.[47] Based on this derived value, relatively more repulsive interactions are then determined. Groot and Warren[47] showed how the χ parameter of the Flory-Huggins theory of concentrated polymer solutions/blends is linearly related to an excess repulsion energy between different polymers. In particular, interactions between different system components are set according to this excess repulsion energy (Δa):[47,62]

$$\chi k_BT = (0.306 \pm 0.003)\Delta a \quad (9)$$

To examine the effect of interfacial segregation between polymers A and B on interfacial width and slip lengths, various χ parameters have been used and the interactions on the different portions of Janus rods, wether they are explicitly grafted or not, have been tuned accordingly.[48] Table 1 illustrates the range of interaction potential parameters that has been studied. The magnitude of graft interactions on different portions of JR are identical to those of JR themselves (J_A and J_B).

3 Results and discussion

In this section, first, equilibrium simulations are reported to extract the width of a flat interface between two segregated polymer phases. This is done for various χ values and polymer chain lengths C. Next, shear flow is applied at a fixed shear rate and the

Table 1 Range of interaction parameters (a_{ij}) in units of $\frac{k_BT}{r_c}$

	A	B	J_A	J_B
A	25	35/50/80	25	40/55/85
B		25	40/55/85	25
J_A			25	40/55/85
J_B				25

effects of χ and C on a calculated slip length and shear interfacial viscosity are evaluated. Then, symmetrically-amphiphilic Janus nanorods and block copolymers of different lengths are added in the system to explore how rigid compatibilizers enhance shear interfacial viscosity. Lastly, this entire analysis is extended and applied to even more complex polymer-grafted Janus nanorods. It is thus expected that the present work may help elucidate the governing physics of nanoparticle interfacial structure and dynamics, which have implications for emulsion stabilization.

3.1 Interfacial width and slip

The interfacial width a_I of fluid-fluid interfaces can be assessed from density profiles across the interface (Equation 10; Figure S1a, ESI†):[21,22,63]

$$\rho_{A,B}(y) = \frac{\rho}{1+e^{\frac{-4y}{a_I}}} \tag{10}$$

As repulsion between phases gets stronger, the interface sharpens only slightly and is independent of polymer molar mass. This is shown in Figure 2 along with density profiles.

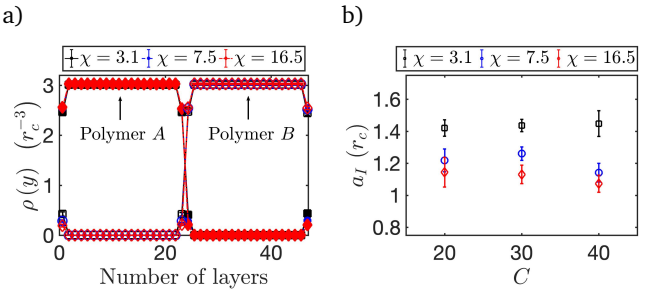

Fig. 2 a) Density profiles across the interface as a function of χ ($C = 20$); and b) interfacial width as a function of C and χ. Error bars are based on standard deviation calculations.

To quantitatively assess slip and interfacial viscosity, average particle velocities in the x (flow) direction ($V_x(y)$) are measured analogously to density profiles (Figure S2, ESI†). Shear stresses $\sigma_{xy}(t)$ in polymeric systems can be measured from chain stretching and orientation:[52,64,65] $\sigma(t) = 3k_BT\rho_C\sum_{c_p=1}^{C}\upsilon(c_p,t)^2\mathbf{S}'(c_p,t)$, where $\sigma(t)$ is the stress at a given time t; ρ_C is the number density of a monodisperse system of polymer chains of length C; the sum runs for each sub-chain unit c_p (polymer particle) in a given chain; $\upsilon(c_p,t)$ is a bond stretch ratio; and $\mathbf{S}'(c_p,t)$ is a local orientation tensor describing orientational anisotropy.[52,64,65] For coarse-grained systems of monodisperse polymer blends, this expression holds both for the blend as a whole – an ensemble mean stress – and also for individual chains in the linear viscoelastic regime.[64]

Slip manifests itself as a region of lower viscosity where the interface is located. This can be seen in Figure 3 from average particle velocities and from stress profiles throughout the calculation box/across the interface. The slightly higher bulk stresses for longer polymer chains are expected as the zero-shear Rouse viscosity η_R scales with polymer molar mass.[66] Therefore, even though the onset of shear-thinning may move to lower shear rates as C increases,[21,67,68] the utilized shear rate is likely sufficiently low to be within or at least close to a Newtonian plateau regime.

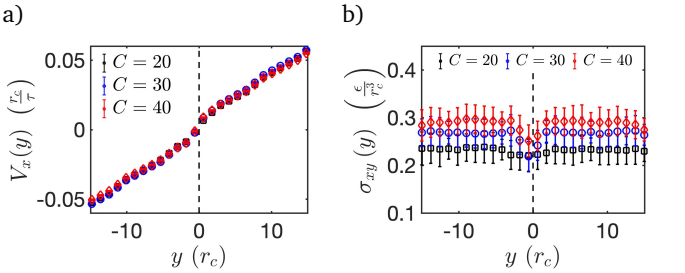

Fig. 3 a) Average particle velocities in the x direction as a function of polymer chain length C ($\chi = 16.5$); and b) shear stress profiles across the interface ($\chi = 3.1$). Error bars in all plots are based on standard deviation calculations. Dashed lines at $y = 0$ indicate where the interface was initially generated in the simulations.

Notably, shear stresses are slightly lower at the interface when polymer chains are longer (Figure 3b). From the predictions by de Gennes and coworkers[16–20], this indicates that shear interfacial viscosity η_I has not become saturated for $C = 20$ and is still limited by polymer chain/loop lengths that enter the interfacial region. It is only in the limit of $R_g > a_I$, where R_g is the chain radius of gyration, that interfacial loop length dictates η_I. In this limit, η_I remains constant irrespective of the increase in C and this limit can be reached once χ is high enough, as shown in Figure 4a. More specifically, it is only at higher χ and $a_I \approx 1.15\ r_c$ (Figure 2) that bulk polymer chain lengths of 20 $\left(\left\langle R_{g,\,C=20}\right\rangle \approx 1.73\ r_c\right)$ are already sufficiently long to yield C-independent η_I values. According to barskey and Robbins,[21] this should happen when R_g of bulk chains exceeds $\approx 1.5a_I$, which is in excellent agreement with the present work ($1.5 \times a_I = 1.5 \times 1.15 = 1.73\ r_c$; $\left\langle R_{g,\,C=20}\right\rangle = 1.73\ r_c$).

A slip length S can furthermore be calculated:[21] $S = \frac{\Delta V}{\dot{\gamma}_B}$, where ΔV represents the velocity jump at the interface and $\dot{\gamma}_B$ is the bulk shear rate. An increase in S is seen mainly as C increases and S does not vary significantly with χ (Figure 4b). Trends relative to interfacial properties and associated discussions illustrate how the present model captures various dynamical aspects of polymer-polymer or fluid-fluid interfaces that have been previously observed with other techniques.[21,22,69,70] This serves as a very important benchmarking study as no DPD reports are to be found. In the next section, the effect of various state-of-the-art compatibilizers on this apparent velocity "jump" at the interface is analyzed.

3.2 Slip suppression and momentum transfer across the interface

Slip suppression can indeed be verified for sufficiently long surfactants at lower concentrations at the interface (Figure 5a). These

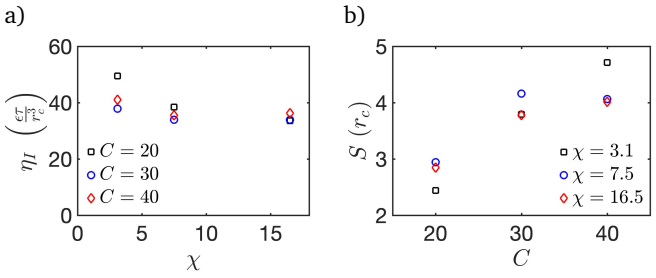

Fig. 4 Interfacial viscosity as a function of χ and C; and b) Calculated slip lengths S as a function of C and χ.

sufficiently long surfactants, at higher concentrations, compose a layer of effectively higher viscosity that decreases the local shear rate at the interfacial level (Figure 5b). Therefore, extant long compatibilizers modify the width of the interfacial region (Figure S3a,b; ESI†) and contribute to enhanced energy dissipation rates and less efficient momentum transfer between polymer phases.

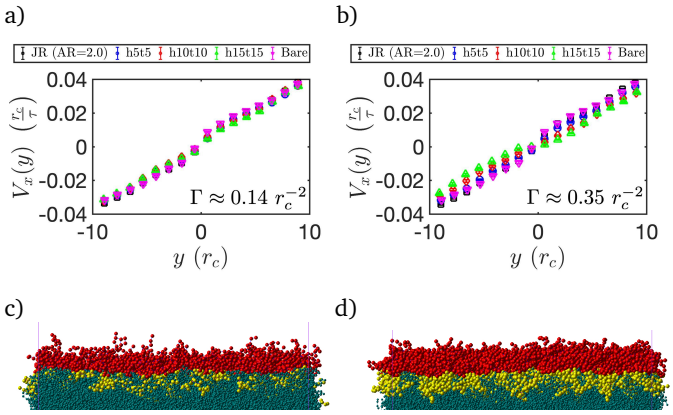

Fig. 5 Velocity profiles in the x (flow) direction as a function of compatibilizer type and corresponding simulation snapshots of the interfacial region for different interfacial concentrations Γ ($\chi = 16.5$; $C = 40$; $s = 2$): a,c) $\Gamma \approx 0.14\ r_c^{-2}$; b,d) $\Gamma \approx 0.35\ r_c^{-2}$. The interfacial plane is located at $y = 0$. Error bars are based on standard deviation calculations.

Because the present work aims to investigate the role of complex surfactants in effectively suppressing slip and mediating momentum transfer across the interface, addressing the fact that momentum and mass diffusivities in DPD are intrinsically coupled is important.[47] Therefore, trends regarding momentum transfer are assessed for standard/commonly-used DPD parameters and also for modified weight functions to efficiently increase Sc or the ratio between momentum and mass diffusivities.[71] Modifying s in Equation 6 is a computationally-efficient way to raise Sc because $Sc \sim r_c^8$. Thus, increasing r_c makes computing time increase rapidly[59] and using a higher γ may require smaller simulation time steps.[47,49] Chen *et al.*[72] and Fan *et al.*[73] chose an exponent $s = \frac{1}{2}$ to raise Sc by a factor of 35. In fact, this also allowed Chen *et al.*[72] to reproduce with DPD the experimentally-observed tumbling behavior of a polymeric droplet upon flow reversal.[74,75] Gidituri *et al.*[76] also recently elected $s = \frac{1}{2}$ for studying Schmidt number effects in their multiphase system. Hence calculations have been carried out both for $s = 2$ and $s = \frac{1}{2}$ as lower s values may allow for gradient discontinuity in the weight function force profile near $\frac{r}{r_c} = 1$.[73] It has been found that the behavior verified in Figure 5 is unaffected whether $s = 2$ or $s = \frac{1}{2}$ is used (Figure S3,c,d; ESI†). Furthermore, these effects have also already been observed directly or indirectly with other simulation techniques,[22,28,29] similar to trends in Figure 4. These remarks suggest that trends in Figure 5 can be reproduced even when mass diffusion is made slower compared to momentum transfer.

Relatively short Janus rods (AR=2.0) in Figure 5 are not effective at suppressing slip and compatibilizer size/length is key in contributing to shear interfacial viscosity. Therefore, an effort is made to make longer Janus rods (AR=4.0) attain a standing orientation at the interface. These longer Janus rods normally attain a tilted/lying configuration,[57] which is also the case for the set of parameters in Table 1. In particular, the interfacial tension between polymer phases has to be decreased[77] and the more repulsive Janus-polymer interactions of Table 1 have to be used concomitantly. Table 2 illustrates the set of DPD parameters that allow for standing Janus rods at the interface with AR=4.0. Namely, a lower interaction parameter $a_{AB} = a_{BA} = 35$ has to necessarily be used and polymer chain sizes have to be restricted to $C = 20$. This set of parameters enables an effective reduction of interfacial tension (lower χC)[47,48] and, finally, an upright configuration for these longer Janus rods (AR=4.0).

Table 2 Interaction parameters (a_{ij}) in units of $\frac{k_B T}{r_c}$ that yield standing Janus rods with AR=4.0 at the interface

	A	B	J_A	J_B
A	25	35	25	85
B		25	85	25
J_A			25	85
J_B				25

Longer Janus rods (AR=4.0) penetrate into the polymer phases as much as flexible surfactants of the h5t5 type ($R_g \approx 1.45$), as depicted in Figure 6a. The higher particle density on the rod; the unfavorable interactions that follow; and their corresponding orientation during flow (Figure 6b) impart a slightly higher – or at least comparable – shear viscosity at the interface (Figure 6c,d). The slightly lower stresses for Janus rods (Figure 6d) arise because there is no contribution from bond stretching ($\upsilon(c_p,t)$ is always unity) as there is, for example, in h10t10/h15t15 diblock copolymers. The orientational contribution $\mathbf{S}'(c_p,t)$ may also be slightly lower because of their aggregation behavior. Clearly, however, the extent of penetration into the polymer phases is correlated with a lower interfacial shear rate (Figure 6a,c) and successful slip suppression for Janus rods. Guo *et al.*[28] correlated the enhanced shear interfacial viscosity provided by block copolymers with their orientation degree and that of bulk/interfacial homopolymers. They showed how interfacial homopolymers at a bare interface are easier to orient/deform because of extant more repulsive interactions.[28] By minimizing these unfavorable interactions with compatibilizers that are not as easily oriented at the interface, this higher viscosity manifests at the interface.[28] Analogously, the higher particle density on JR may contribute to a lower polymer penetration into the interfacial region as they

are essentially solid objects,. From density profiles, however, this effect from JR rigidity is unimportant (Figures S3 and S4; ESI†). Therefore, effects verified by Guo *et al.* [28] according to the present work, also depend on surfactant length, rigidity, interface width or how depleted the interface is from homopolymers (Figures S3 and S4; ESI†).

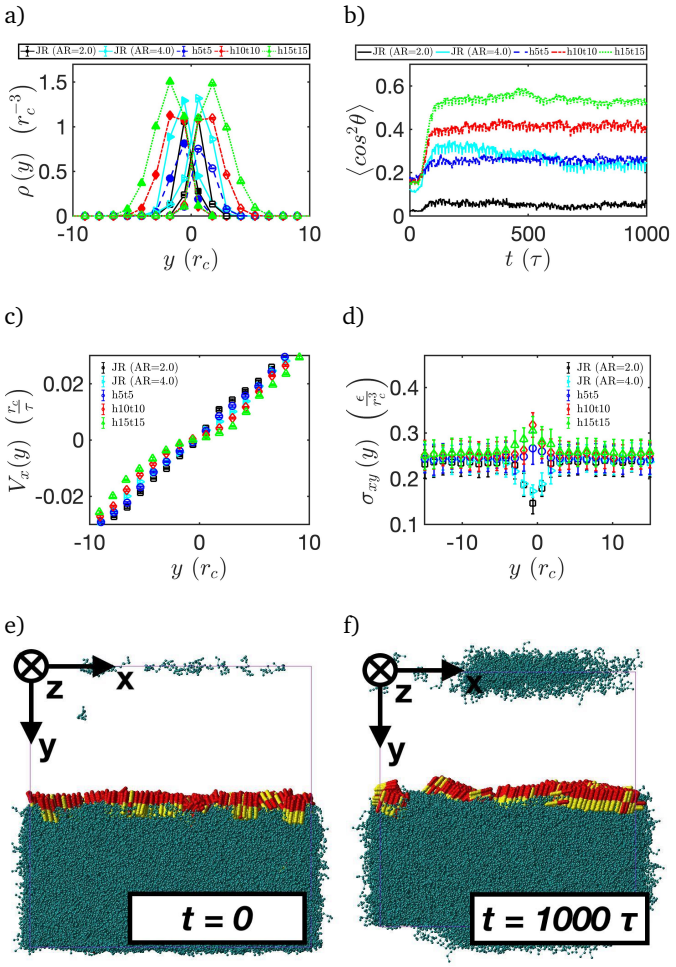

Fig. 6 a) Density profiles for different surfactant portions: head (solid symbols) and tail (empty symbols) groups; b) ensemble mean orientation of compatibilizers in the flow direction during shear flow; c) Velocity profiles in the x (flow) direction; d) shear stresses across the y direction; e) system snapshot (JR; AR=4.0) right before shear is applied; and f) at the end of shear. Error bars in a), c), and d) are based on standard deviation calculations and lines in a) are simply for guiding the eye. The interfacial plane is located at $y = 0$. All plots correspond to $\Gamma \approx 0.35\ r_c^{-2}$; $C = 20$ (Table 2).

To fairly compare compatibilizers with the same mass in terms of density of favorable/unfavorable interactions, Janus nanorods (AR=2.0) are subsequently grafted with flexible polymer chains to make up for a maximum of 30 DPD particles. This maximum surfactant mass/size in the form of density of interactions is equivalent to h15t15 compatibilizers that contribute the least efficiently to momentum transfer in Figure 6. The distribution of chains along JR – grafting density – and/or their length may dictate interfacial width and/or aggregation for example.[57] To explore the entropic and enthalpic effects from grafting Janus nanorods with ligands/polymers[37] and their impact on (i) slip suppression; (ii) momentum transfer; and (iii) 2D interfacial microstructure, in the next section, results with regard to polymer-grafted Janus nanorods are discussed.

3.3 Polymer-grafted Janus rods: effects of chain length and grafting density

In this section, Janus rods (AR=2.0) are symmetrically grafted with 20 DPD particles to make up surfactants with the same mass/density of interactions as h15t15, which affect shear interfacial viscosity most significantly in Figure 6c,d. The degree of polymerization of homopolymers; the repulsion between them; and surfactant interfacial concentration are kept constant ($C = 20$; $\chi = 3.1$; $\Gamma \approx 0.35\ r_c^{-2}$) and identical to Figure 6 and Table 2.

3.3.1 Equilibrium interfacial microstructure

As studied by Paiva *et al.*,[57] short JR (AR=2.0) form liquid crystalline-like aggregates at the interface with a standing orientation. It is thus expected that, when grafted with polymer chains/ligands, depending on N_g or L_g, their structure is affected. From 2D radial distribution functions from the centers of mass of the rigid part of polymer-grafted JR, some degree of short/long-range order or crystallinity can be seen for $N_g = 2$ and $L_g = 1$; $N_g = 2$ and $L_g = 2$; and essentially only for these sets of parameters (Figure 7). Increasing grafting density is more efficient at dispersing JR.

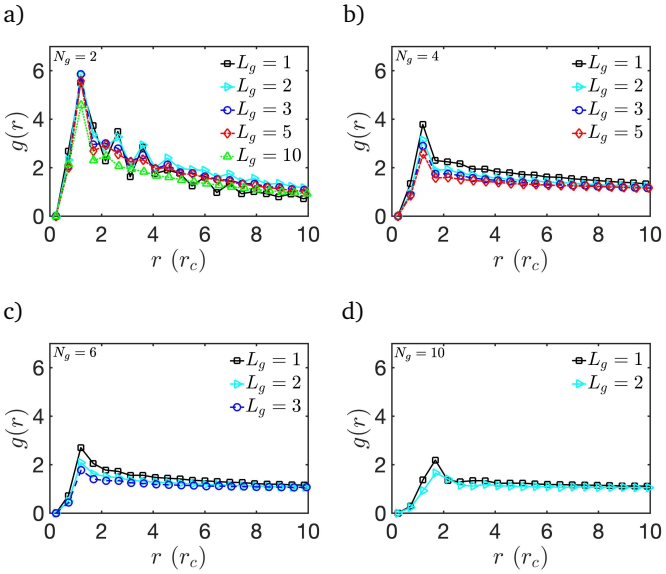

Fig. 7 2D radial distribution functions as measured with respect to the center of mass of the rigid portion of polymer-grafted JR as a function of graft chain length L_g for: a) $N_g = 2$; b) $N_g = 4$; c) $N_g = 6$; d) $N_g = 10$.

Increasing graft length L_g makes JR less oriented in the direction of the interface normal (Figure 8a). As L_g increases, the increase in $\langle \cos^2 \theta \rangle$ reflects the disruption of aggregates or liquid crystalline-like domains seen in Figure 7. Moreover, as the rigid portion of Janus surfactants is progressively freed from these aggregates, instead of diffusing more slowly as L_g increases, larger particles diffuse faster in view of a less pronounced "caging" ef-

fect (Figure 8b).[57] It is only at high grafting densities, for which aggregate structure is more completely disrupted (Figure 7), that the centers of mass of JR experience enhanced drag from graft particles and diffuse slower as L_g increases (Figure 8b). This also ultimately affects their orientation at $N_g = 10$ (Figure 8a). The more ordered aggregate structures (Figure 7) are also consistent with a more upright orientation and slower diffusion in absolute terms (Figure 8). In fact, the center of mass of the rigid portion of polymer-grafted JR is always diffusing faster than graft-free JR (Figure S5, ESI†), which confirms a certain degree of aggregate disruption.

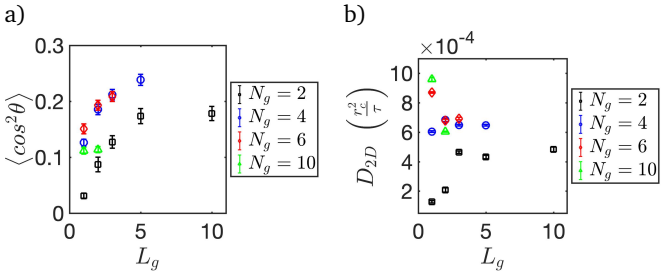

Fig. 8 a) Ensemble mean orientation of the rigid portion of polymer-grafted JR and b) ensemble mean 2D diffusion coefficient with respect to the center of mass of the rigid portion of polymer-grafted JR as a function of L_g and N_g. Error bars are based on standard deviation calculations.

It is apparent that increasing the number of grafts on JR allows for more lateral interactions (Figure 9). Most notably, a relatively dense 2D film can be seen for $N_g = 10$; $L_g = 2$ and individual surfactants with the same number of DPD particles (blue dashed frames in Figure 9) present 2D mesophases of lower fractal dimension. This is relevant from at least two viewpoints: (i) firstly, de Gennes[30] highlighted in his Nobel lecture that the films formed by Janus particles could potentially enable tunable pore structures and allow chemical exchange across the interface. This is similar to what is observed in Figure 9. It also illustrates the technological potential of the present work for surfactant design regarding controlled nanoparticle aggregation through graft number/length. This interfacial feature of Janus particles is overlooked in the literature as most studies focus on their capabilities to decrease interfacial tension. Moreover, it differs from the corresponding random distribution of flexible block copolymers at the interface (Figure S6, ESI†). Intermediate grafting densities/length are predicted to most easily enable well-controlled pore structures to be formed in Figure 10; (ii) secondly, Figure 10 indicates that grafts penetrate the homopolymer phases when they are made longer, instead of for example increasingly dispersing the rods at the interfacial plane.[37] Therefore, graft length is expected to play an important role in mediating momentum transfer. These aspects will be addressed next.

3.3.2 Impact on momentum transfer

The fact that sufficiently-long grafts are necessary to penetrate homopolymer phases is supported by density profiles in Figure 10a,b,c,d. The interface becomes wider for a low $\frac{N_g}{L_g}$ ratio. Sufficiently-long grafts ($L_g > 5; 10$) indeed impact how efficiently momentum is transferred between phases, as can be seen in Figure 10e,f,g,h. This suggests that interpenetration is highly correlated with "friction"/energy dissipation rates when shear flow is applied. Hence, at constant interfacial interaction density, longer grafts should be preferred when this effect is desired.

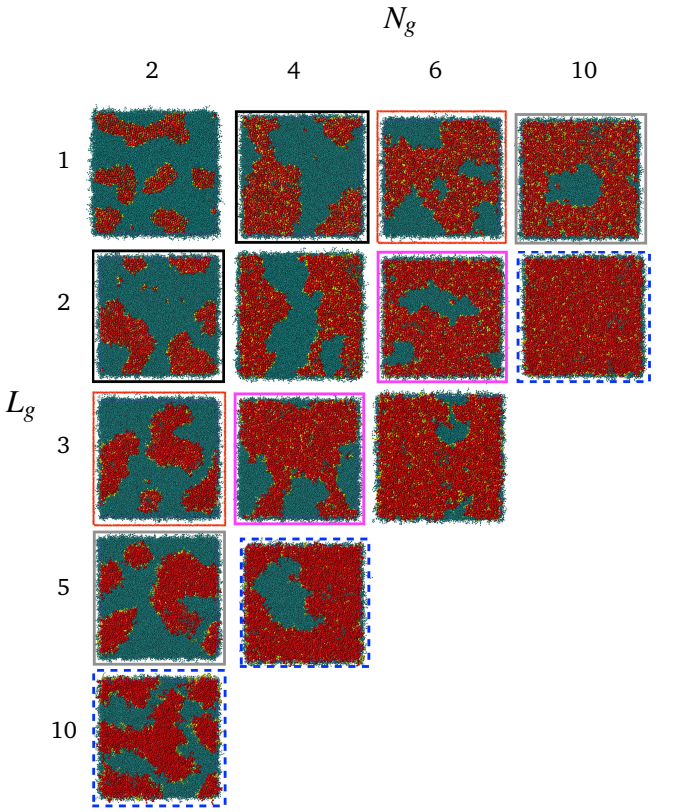

Fig. 9 Equilibrium snapshots (top views) from simulation boxes showing the entire interfacial region as a function of L_g and N_g. Solid or dashed-line frames around snapshots are color-coded amongst themselves to highlight systems with surfactants that are composed of the same number of DPD particles (whilst different L_g and N_g values).

Sagis *et al.*[29] showed very recently that a momentum transfer mechanism could explain dynamic heterogeneities at complex interfaces. The authors calculated a momentum transfer coefficient ξ_{xx} from shear stress measurements; interfacial velocities V_x^I; and extrapolated bulk velocities (V_x^E). Thus, ξ_{xx} can be extracted from Equation 11:

$$\sigma_{xy} = \xi_{xx}\left(V_x^E - V_x^I\right) \tag{11}$$

where V_x^I is herein taken to be 0 in the present work within a Gibbs dividing surface framework ($y = 0$).[29,78–81] In Equation 11, the bulk phases are assumed to have equal viscosities and densities and to behave as Newtonian liquids.[29] It also should hold only for symmetrically amphiphilic surfactants and this is the reason why only symmetric ones have been utilized. Additionally, ξ_{xx} can be normalized by the bulk viscosity of polymeric phases to yield a characteristic length scale δ, often termed as "friction" thickness.[22,82] It can be interpreted as how well hydrodynamic flow penetrates into the interfacial region[22] and is analogous to the hydrodynamic penetration depth from polymer brush theory.[83] To account for slight differences in bulk/interface shear

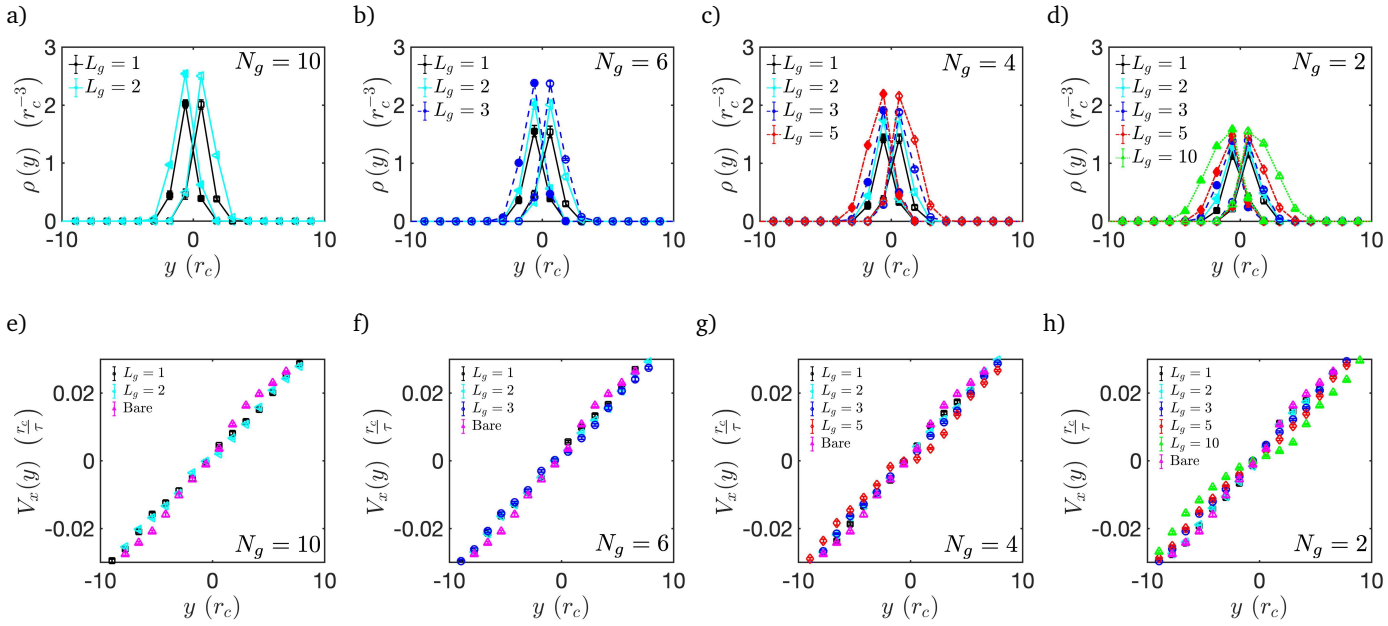

Fig. 10 Density profiles for the different surfactant portions: head (solid symbols) and tail (empty symbols) groups; and velocity profiles in the x (flow) directionas a function of graft chain length L_g for: a,e) $N_g = 10$; b,f) $N_g = 6$; c,g) $N_g = 4$; d,h) $N_g = 2$. Error bars are based on standard deviation calculations. The interfacial plane is located at $y = 0$.

stresses (Figures 6 and S7, ESI†), an ensemble mean steady-state shear stress has been used in Equation 11 to compute δ and a shear interfacial viscosity η_I has been calculated separately from interfacial shear stresses and shear rates (Figure S7, ESI†). Moreover, to unite distinct measures of surfactant size (rod length, graft chain size, copolymer chain size) into a single parameter and assess the degree of interpenetration with polymer phases, a penetration height h has been calculated from compatibilizer density profiles (Equation 12):[84,85]

$$h = \frac{\int_{-L_y/2}^{L_y/2} y\,\rho(y)\,dy}{\int_{-L_y/2}^{L_y/2} \rho(y)\,dy} \tag{12}$$

Moreover, a Boussinesq number Bo can be calculated according to Fuller and Vermant:[86] $Bo = \frac{\eta_I}{\eta L}$, where η is the bulk viscosity; and L is a characteristic length scale appropriate to the geometry of a given problem.[86] Herein, L is taken to be the interpenetration height h as this parameter provides information on interfacial wetting by bulk phases or on interfacial area/perimeter ratio. Thus, interpenetration between interfacial material and the matrix phases would correlate with L as it is important for sensitivity of rheometric measurements.[86] It would also dictate line tension effects experimentally, for example.[86] A particle Stokes number St has also been calculated to illustrate how inertial forces are negligible compared to viscous forces (ESI†): $St = \mathcal{O}(10^{-5})$ for all compatibilizers.[87]

If the interfacial activity of nanoparticles can be guaranteed[88] and polymeric emulsion stabilization is targeted, it is suggested that sparsely grafted Janus nanorods with long grafts be employed. They contribute to very low δ or very little flow penetration into the interfacial layer, much like h15t15 diblock copolymers (Figure 11a). The role of enhanced energy dissipation rates at an interfacial level is illustrated by a power law correlation $\xi_{xx} \sim Bo^{-1.43\pm0.77}$ in Figure 11b. This higher Bo could delay film drainage times between two approaching polymeric droplets and their coalescence.[22] Less efficient momentum transfer across the interface helps stabilize polymer blend droplet morphology systems in which interfacial curvature is not relevant.[22,24–27] In this context, findings herein provide a molecular picture that could guide studies on Janus particles under processing-like conditions, such as the promising one by Bahrami *et al.*[89] Even though nanoparticles in the present work are referred to as polymer-grafted Janus rods, the underlying physics is expected to be the same for symmetric bottlebrush block copolymers possessing a rigid backbone.[90,91]

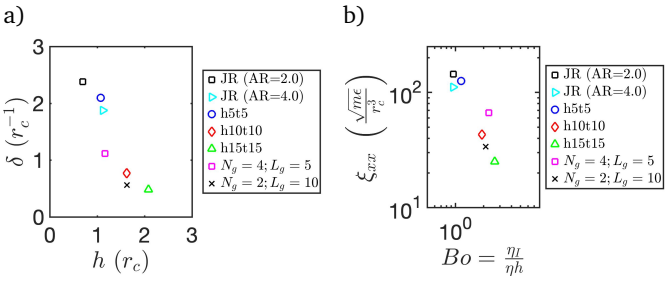

Fig. 11 a) "Friction" thickness δ as a function of compatibilizer penetration degree h and compatibilizer type; and b) power law scaling relationship between momentum transfer coefficient ξ_{xx} and Boussinesq number Bo.

Alternately, results in Figure 11 could also help explain trends in film rupture experiments, such as those performed by Borrel and Leal.[35] Namely, nanoparticles were observed to favor coalescence in spite of promoting lower interfacial tension.[35] Length scales in those experiments are well within those acces-

sible with DPD and molecular simulations. Namely, from previously published work using the present polymer blend model,[48] a typical length scale is $r_c = 1.06\,\text{nm}$ with nanorod length of $\approx 2.0\,\text{nm}$ (AR=2.0) and the ensemble mean ligand radius of gyration herein is $\langle R_{g,l} \rangle \approx 1.2\, r_c \approx 1.3\,\text{nm}$ when $L_g = 10$. In Borrell and Leal,[35] the radius of nanoparticles and $\langle R_{g,l} \rangle$ were respectively 1.5 nm and 2.0 nm.[34,35] The experiments by Borrell and Leal[35] would also be applicable to simulated flat interfaces with zero curvature, given droplet sizes are much larger than characteristic molecular length scales at the interface.[35]

Effects from nanoparticle interfacial diffusivity are nontrivial (Figure 8) even if, according to Vannozzi,[34] they may help explain reductions in film drainage time. A shear interfacial viscosity or momentum transfer mechanism was not considered by Vannozzi[34] to explain the experiments by Borrell and Leal[35] because of typically small *Bo* arising from the high bulk viscosity of polymers.[34,86,92,93] This makes it difficult to distinguish the effect of polymer-grafted nanoparticles on shear interfacial viscosity in immiscible polymer blends from that of bulk viscosity.[34,86] This is, therefore, another aspect to which the present work contributes (Figure 11).

In the work by Zhao and Macosko,[1] slip across dozens of polymer-polymer interfaces resulted in lower apparent viscosity measurements. This can be controlled with block copolymers, as noted by the authors.[1] However, if Janus particles with long grafts are used, comparable momentum transfer effects (Figure 11) and better control over interfacial microstructure can be achieved from nanoparticle aggregation (Figure 9). Therefore, this could potentially allow for controllable porous structures that could mediate chemical exchange[30] in a direction that is perpendicular to the interfacial plane.

As another example, placing nanoparticles at the interface between polymer layers and controlling their spacing through grafting density (Figures 7 and 9) may enhance the efficiency of polymer solar cells based on plasmonics arguments.[94–96] The fact that specifically dynamic, shear flow aspects are unveiled in Figure 11 helps elucidate what could be more efficient ways of fabricating/processing these devices.

Finally, the rich dynamic colloidal behavior observed by Paiva *et al.*[48] using the same JR model is associated thus with a "friction" thickness of order of the nanorod length ($\delta \approx 2.4\, r_c$; Figure 11), which illustrates how hydrodynamic flow penetrates well within the interfacial region and directs intricate nanorod assemblies.[48] Ongoing work consists of extending this study to entangled polymer blend systems.[51,52]

4 Conclusions

Interfacial slip or adhesion of polymer-polymer interfaces impacts polymer blend compatibilization operations. This is specially relevant for multiphase nanomaterials with a more significant amount of interfacial area. Under processing conditions as in coextruded systems with thousands of polymer layers, interfacial components may effectively multiply and exacerbate these effects that would be otherwise negligible macroscopically. The present model has been successfully benchmarked with physical scaling relationships that apply to unentangled polymer blend interfaces subject to interfacial slip under tangential shear flow. It has then been applied to more complex polymer-polymer interfaces.

In that sense, grafting nanoparticles with polymers offers useful degrees of freedom that can be used to tune 2D interfacial morphology. Increasing grafting density was a more efficient and effective parameter for dispersing Janus rods at the interface than their corresponding graft length. Making grafts longer directs interpenetration with polymer phases and dictates the extent to which momentum is transferred across the interface. The orientation of longer, graft-free Janus rods has been tuned from a tilted to an upright configuration to illustrate this effect. Hence, interfacial width/penetration was key in determining conditions for which interfacial rheological properties are comparable between Janus particles and block copolymer analogs. Under tangential shear flow conditions, Janus rods are able to mediate momentum transfer across the interface or suppress slip as efficiently as these diblock copolymers. Given that Janus particles are commonly more interfacially active than flexible block copolymer surfactants and normally reduce interfacial tension to a greater extent, these findings more closely unveil mechanisms through which nanoparticles may or may not excel at emulsion stabilization/polymer blend compatibilization.

Conflicts of interest

There are no conflicts to declare.

Acknowledgements

This study was financed in part by the Coordenação de Aperfeiçoamento de Pessoal de Nível Superior - Brasil (CAPES) - Finance Code 001. The authors also acknowledge funding from the National Science Foundation via grant #CBET-1703919. This work made use of the High Performance Computing Resource in the Core Facility for Advanced Research Computing at Case Western Reserve University.

References

1 R. Zhao and C. W. Macosko, *Journal of Rheology*, 2002, **46**, 145–167.
2 K. B. Migler, C. Lavallée, M. P. Dillon, S. S. Woods and C. L. Gettinger, *Journal of Rheology*, 2001, **45**, 565–581.
3 J. Zhang, T. P. Lodge and C. W. Macosko, *Journal of Rheology*, 2006, **50**, 41–57.
4 H. Zeng, Y. Tian, B. Zhao, M. Tirrell and J. Israelachvili, *Langmuir*, 2009, **25**, 4954–4964.
5 G. D. Zartman and S. Q. Wang, *Macromolecules*, 2011, **44**, 9814–9820.
6 Y. C. Lam, L. Jiang, C. Y. Yue, K. C. Tam, L. Li and X. Hu, *Journal of Rheology*, 2003, **47**, 795–807.
7 P. C. Lee and C. W. Macosko, *Journal of Rheology*, 2010, **54**, 1207–1218.
8 P. C. Lee, H. E. Park, D. C. Morse and C. W. Macosko, *Journal of Rheology*, 2009, **53**, 893–915.
9 M. Urbakh and E. Meyer, *Nature Materials*, 2010, **9**, 8–10.
10 B. Bhushan, J. N. Israelachvili and U. Landman, *Nature*, 1995, **374**, 607–616.

11 S.-p. Zhan, H. Xu, H.-t. Duan, L. Pan, D. Jia, J. Tu, L. Liu and J. Li, *Soft Matter*, 2019, **15**, 8827–8839.

12 E. Andablo-Reyes, D. Yerani, M. Fu, E. Liamas, S. Connell, O. Torres and A. Sarkar, *Soft Matter*, 2019, **15**, 9614–9624.

13 C.-c. Chang, I. Williams, A. Nowbahar, V. Mansard, J. Mecca, K. A. Whitaker, A. K. Schmitt, C. J. Tucker, T. H. Kalantar, T.-c. Kuo and T. M. Squires, *Langmuir*, 2019, acs.langmuir.9b00834.

14 Y. Li, J. Xu and D. Li, *Microfluidics and Nanofluidics*, 2010, **9**, 1011–1031.

15 C. Zhao, J. E. Sprittles and D. A. Lockerby, *Journal of Fluid Mechanics*, 2019, **861**, R3.

16 P.-G. De Gennes, *Scaling Concepts in Polymer Physics*, Cornell University Press, 1st edn, 1979.

17 F. Brochard-Wyart, P.-G. de Gennes and S. Troian, *Comptes rendus de l'Académie des sciences*, 1990, **310**, 1169–1173.

18 F. Brochard and P. G. De Gennes, *Langmuir*, 1992, **8**, 3033–3037.

19 P.-G. de Gennes, *Physics of polymer surfaces and interfaces*, Butterworth-Heinemann, 1992, ch. 3, pp. 55–71.

20 J. Goveas and G. Fredrickson, *The European Physical Journal B*, 1998, **2**, 79–92.

21 S. Barsky and M. O. Robbins, *Physical Review E - Statistical, Nonlinear, and Soft Matter Physics*, 2001, **63**, 1–7.

22 B. Narayanan, V. A. Pryamitsyn and V. Ganesan, *Macromolecules*, 2004, **37**, 10180–10194.

23 Y. Hu, X. Zhang and W. Wang, *Langmuir*, 2010, **26**, 10693–10702.

24 S. P. Lyu, *Macromolecules*, 2003, **36**, 10052–10055.

25 S. P. Lyu, T. D. Jones, F. S. Bates and C. W. Macosko, *Macromolecules*, 2002, **35**, 7845–7855.

26 Y. Gong and L. G. Leal, *Journal of Rheology*, 2012, **56**, 397–433.

27 J. Genoyer, J. Soulestin and N. R. Demarquette, *Journal of Rheology*, 2018, **62**, 681–693.

28 R. Guo, J. Li, L.-T. Yan and X.-M. Xie, *Soft Matter*, 2013, **9**, 255–260.

29 L. M. C. Sagis, B. Liu, Y. Li, J. Essers, J. Yang, A. Moghimikheirabadi, E. Hinderink, C. Berton-Carabin and K. Schroen, *Scientific Reports*, 2019, **9**, 2938.

30 P.-G. De Gennes, *Angewandte Chemie International Edition in English*, 1992, **31**, 842–845.

31 B. P. Binks and P. D. I. Fletcher, *Langmuir*, 2001, **17**, 4708–4710.

32 Q. Li, L. Wang, J. Lin and L. Zhang, *Physical Chemistry Chemical Physics*, 2019, **21**, 2651–2658.

33 S. Razavi, L. M. Hernandez, A. Read, W. L. Vargas and I. Kretzschmar, *Journal of Colloid and Interface Science*, 2020, **558**, 95–99.

34 C. Vannozzi, *Physics of Fluids*, 2019, **31**, 082112.

35 M. Borrell and L. G. Leal, *Langmuir*, 2007, **23**, 12497–12502.

36 R. Cardinaels, *Compatibilization of Polymer Blends*, Elsevier, 2020, pp. 249–275.

37 S. Khani, S. Jamali, A. Boromand, M. J. A. Hore and J. Maia, *Soft Matter*, 2015, **11**, 6881–6892.

38 J. Shen, X. Li, X. Shen and J. Liu, *Macromolecules*, 2017, **50**, 687–699.

39 V. Gollanapalli, A. Manthri, U. K. Sankar and M. Tripathy, *Macromolecules*, 2017, **50**, 8816–8826.

40 Y. Chen, Q. Xu, Y. Jin, X. Qian, L. Liu, J. Liu and V. Ganesan, *Macromolecules*, 2018, **51**, 4143–4157.

41 M. J. Hore and R. J. Composto, *Current Opinion in Chemical Engineering*, 2013, **2**, 95–102.

42 P. J. Hoogerbrugge and J. M. V. A. Koelman, *Europhysics Letters (EPL)*, 1992, **19**, 155–160.

43 J. M. V. A. Koelman and P. J. Hoogerbrugge, *Europhysics Letters (EPL)*, 1993, **21**, 363–368.

44 P. Español, *Physical Review E*, 1995, **52**, 1734–1742.

45 P. Español and P. Warren, *Europhysics Letters (EPL)*, 1995, **30**, 191–196.

46 M. P. Allen and D. J. Tildesley, *Computer Simulation of Liquids*, Oxford University Press, 1989.

47 R. D. Groot and P. B. Warren, *The Journal of Chemical Physics*, 1997, **107**, 4423–4435.

48 F. L. Paiva, M. J. A. Hore, A. Secchi, V. Calado, J. Maia and S. Khani, *Langmuir*, 2020, **36**, 4184–4193.

49 A. Boromand, S. Jamali and J. M. Maia, *Computer Physics Communications*, 2015, **196**, 149–160.

50 A. W. Lees and S. F. Edwards, *Journal of Physics C: Solid State Physics*, 1972, **5**, 1921–1928.

51 M. Yamanoi, O. Pozo and J. M. Maia, *The Journal of Chemical Physics*, 2011, **135**, 044904.

52 S. Khani, M. Yamanoi and J. Maia, *The Journal of Chemical Physics*, 2013, **138**, 174903.

53 S. Jamali, M. Yamanoi and J. Maia, *Soft Matter*, 2013, **9**, 1506–1515.

54 S. Jamali, A. Boromand, N. Wagner and J. Maia, *Journal of Rheology*, 2015, **59**, 1377–1395.

55 S. Jamali, A. Boromand, S. Khani and J. Maia, *Computer Physics Communications*, 2015, **197**, 27–34.

56 A. Boromand, S. Jamali and J. M. Maia, *Soft Matter*, 2017, **13**, 458–473.

57 F. Paiva, A. Boromand, J. Maia, A. Secchi, V. Calado and S. Khani, *The Journal of Chemical Physics*, 2019, **151**, 114907.

58 E. Cudjoe, S. Khani, A. E. Way, M. J. A. Hore, J. Maia and S. J. Rowan, *ACS Central Science*, 2017, **3**, 886–894.

59 D. Rapaport, *The Art of Molecular Dynamics Simulations*, Cambridge University Press, 2nd edn, 2004.

60 R. M. Choueiri, E. Galati, H. Thérien-Aubin, A. Klinkova, E. M. Larin, A. Querejeta-Fernández, L. Han, H. L. Xin, O. Gang, E. B. Zhulina, M. Rubinstein and E. Kumacheva, *Nature*, 2016, **538**, 79–83.

61 T. Bürgi, *Nanoscale*, 2015, **7**, 15553–15567.

62 S. Jamali, A. Boromand, S. Khani, J. Wagner, M. Yamanoi and J. Maia, *The Journal of Chemical Physics*, 2015, **142**, 164902.

63 E. Helfand and Y. Tagami, *The Journal of Chemical Physics*, 1972, **56**, 3592–3601.

64 H. Watanabe, *Progress in Polymer Science (Oxford)*, 1999, **24**, 1253–1403.

65 M. Doi and S. Edwards, *The theory of polymer dynamics*, Clarendon Press, 1986.

66 M. Rubinstein and R. Colby, *Polymer Physics*, Oxford University Press, 2003.

67 Z. Xu, J. J. De Pablo and S. Kim, *The Journal of Chemical Physics*, 1995, **102**, 5836–5844.

68 R. Khare, J. J. De Pablo and A. Yethiraj, *Macromolecules*, 1996, **29**, 7910–7918.

69 J. Koplik and J. R. Banavar, *Physical Review Letters*, 2006, **96**, 2–5.

70 P. Poesio, A. Damone and O. K. Matar, *Physical Review Fluids*, 2017, **2**, 044004.

71 R. C. Krafnick and A. E. García, *The Journal of Chemical Physics*, 2015, **143**, 243106.

72 S. Chen, N. Phan-Thien, X.-J. Fan and B. C. Khoo, *Journal of Non-Newtonian Fluid Mechanics*, 2004, **118**, 65–81.

73 X. Fan, N. Phan-Thien, S. Chen, X. Wu and T. Yong Ng, *Physics of Fluids*, 2006, **18**, 063102.

74 S. Guido, M. Minale and P. L. Maffettone, *Journal of Rheology*, 2000, **44**, 1385–1399.

75 M. Minale, P. Moldenaers and J. Mewis, *Journal of Rheology*, 1999, **43**, 815–827.

76 H. Gidituri, V. S. Akella, S. Vedantam and M. V. Panchagnula, *The Journal of Chemical Physics*, 2019, **150**, 234903.

77 B. J. Park and D. Lee, *ACS Nano*, 2012, **6**, 782–790.

78 L. M. C. Sagis, *Rev. Mod. Phys.*, 2011, **83**, 1367–1403.

79 A. Lamorgese, R. Mauri and L. M. Sagis, *Physics Reports*, 2017, **675**, 1–54.

80 J. Gibbs, *The Collected Works of J. Willard Gibbs, Volume I: Thermodynamics*, Yale University Press, 1928.

81 J. Slattery, L. Sagid and E. Oh, *Interfacial Transport Phenomena*, Springer-Verlag, 2nd edn, 2007.

82 C. Neto, D. R. Evans, E. Bonaccurso, H. J. Butt and V. S. Craig, *Reports on Progress in Physics*, 2005, **68**, 2859–2897.

83 S. T. Milner, *Macromolecules*, 1991, **24**, 3704–3705.

84 F. Goujon, P. Malfreyt and D. J. Tildesley, *The Journal of Chemical Physics*, 2008, **129**, 034902.

85 G. S. Grest, *Macromolecules*, 1994, **27**, 418–426.

86 G. G. Fuller and J. Vermant, *Annual Review of Chemical and Biomolecular Engineering*, 2012, **3**, 519–543.

87 J. Mewis and N. J. Wagner, *Colloidal Suspension Rheology*, Cambridge University Press, 2012.

88 D. L. Cheung and S. A. F. Bon, *Physical Review Letters*, 2009, **102**, 066103.

89 R. Bahrami, T. I. Löbling, A. H. Gröschel, H. Schmalz, A. H. E. Müller and V. Altstädt, *ACS Nano*, 2014, **8**, 10048–10056.

90 A. Chremos and P. E. Theodorakis, *Polymer*, 2016, **97**, 191 – 195.

91 L. Jiang, D. Nykypanchuk, V. J. Pastore and J. Rzayev, *Macromolecules*, 2019, **52**, 8217–8226.

92 D. E. Tambe and M. M. Sharma, *Journal of Colloid and Interface Science*, 1994, **162**, 1 – 10.

93 K. D. Danov, D. S. Valkovska and I. B. Ivanov, *Journal of Colloid and Interface Science*, 1999, **211**, 291 – 303.

94 R. F. Service, *Science*, 2008, **319**, 718–720.

95 M. J. A. Hore and R. J. Composto, *ACS Nano*, 2010, **4**, 6941–6949.

96 M. D. Kelzenberg, S. W. Boettcher, J. A. Petykiewicz, D. B. Turner-Evans, M. C. Putnam, E. L. Warren, J. M. Spurgeon, R. M. Briggs, N. S. Lewis and H. A. Atwater, *Nature Materials*, 2010, **9**, 239–244.

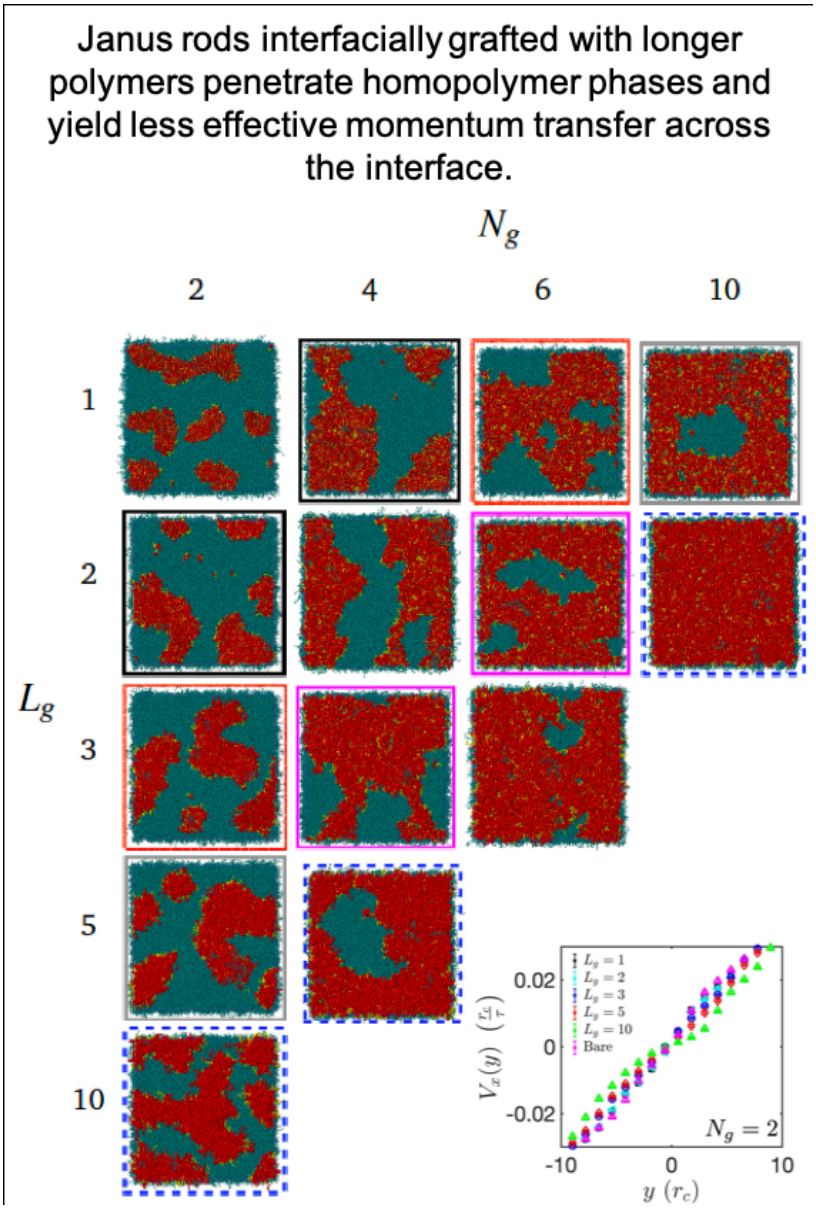
Janus rods interfacially grafted with longer polymers penetrate homopolymer phases and yield less effective momentum transfer across the interface.
N_g
2
4
6
10
L_g
1
2
3
5
10
$L_g = 1$
$L_g = 2$
$L_g = 3$
$L_g = 5$
$L_g = 10$
Bare
$V_x(y)$ $(\frac{r_c}{\tau})$
0.02
0
-0.02
$N_g = 2$
-10
0
10
y (r_c)